UCRL- 95149
PREPRINT

A Time-Dependent Ionization Balance Model for Non-LTE Plasma

Y. T. Lee
G. B. Zimmerman
D. S. Bailey
D. Dickson
D. Kim

This paper was prepared for publication in the Proceedings of the Third International Conference/Workshop on the Radiative Properties of Hot Dense Matter held in Williamsburg, Virginia in October 1985.

May 7, 1986

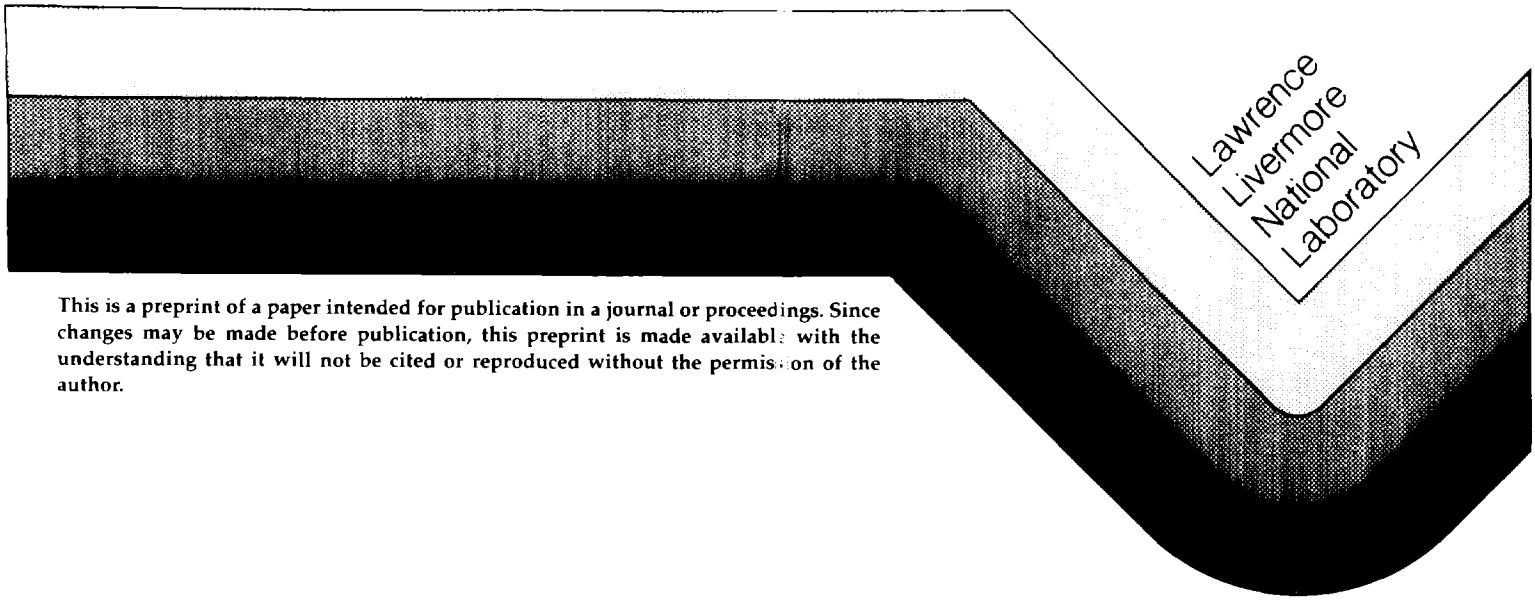

A Time-Dependent Ionization-Balance Model for Non-LTE Plasma*

Y. Lee, G. Zimmerman, D. Bailey,
D. Dickson, and D. Kim

Lawrence Livermore National Laboratory
University of California, Livermore, California 94550

ABSTRACT

We have developed a detailed configuration-accounting kinetic model for calculating time-dependent ionization-balance and ion-level populations in non-local thermal-equilibrium (non-LTE) plasmas. We use these population estimates in computing spectral line intensities, line ratios, and synthetic spectra, and in fitting these calculated values to experimental measurements. The model is also used to design laboratory x-ray laser experiments. For this purpose, it is self-consistently coupled to the hydrodynamics code LASNEX.

---

*Work performed under the auspices of the U. S. Department of Energy by the Lawrence Livermore National Laboratory under contract number W-7405-ENG-48.

I. INTRODUCTION

Many laboratories are actively investigating radiation spectra of plasmas that are produced either by high-power lasers or gas-puff z-pinches, because spectral-line intensities from these plasmas are useful as temperature and density diagnostics. In a well-diagnosed plasma, moreover, information about the emission spectra allows one to test the accuracy of theoretical rate coefficients. Before one can analyze the emission spectra, however, one needs to know the plasma's charge-state distribution and ion-level populations as a function of its electron temperature and density.

Since the plasmas of interest are usually produced with electron densities ranging from 10^{17} to 10^{21} cm^{-3}, neither the coronal nor the Saha-Boltzmann equilibrium can be expected to apply. The Saha-Boltzmann equation, for example, applies only to higher-density plasmas. The coronal model, on the other hand, calculates ionization balance for ions in their ground states, so it applies exclusively to plasmas with electron densities less than 10^{16} cm^{-3}. In this paper we discuss a detailed configuration-accounting kinetic model which can be used in lieu of the coronal and Saha-Boltzmann models to calculate time-dependent ionization balance and ion-level populations of the non-LTE plasmas in the electron-density range of interest.

The model offers two options for calculating ion-level populations. The first (default) option treats all the ionization stages in a plasma in a hydrogenic approximation. The second option treats certain ionization stages in terms of their detailed non-hydrogenic energy levels and rate coefficients.

In the default option, we assume that each energy level couples with every level of the same ionization stage, but only to the ground state of the next ionization stage. (This approximation allows us to develop a particularly efficient method of calculating the populations.) The ground-state and excited-state energy levels for each ionization stage are generated from screening constants. There is one energy level per principal quantum number, and the following processes are included: (1) electron-collisional excitation and de-excitation, (2) radiative emission and absorption, (3) electron-collisional ionization and photoionization, (4) radiative

recombination, (5) three-body recombination, and (6) dielectronic recombination. All the rate coefficients are scaled from those obtained for hydrogenic ions. Using the default option, our model can be used in calculating the charge-state distribution and radiative power of arbitrary non-LTE plasmas.

In the second option, the model retrieves from a data file both the energy levels and the collisional and radiative data for certain ionization stages. The data file includes energy levels, oscillator strengths, collisional excitation- and ionization-rate coefficients, photo-ionization cross sections, and auto-ionization rates. This option allows us to apply the model to the analysis of non-LTE plasma emission spectra and to the simulation of laboratory x-ray laser experiments.

Our model is self-consistently coupled to the hydrodynamic code LASNEX.[1] We use the electron temperature, electron density, and photon density from LASNEX to compute ion-level populations, and these values are then used in the calculation of the average ionization state, emissivity, photon-absorption cross section, and binding energy. LASNEX introduces these quantities into the equations of radiation transport, hydrodynamics, electron energy, and number balance, and thus updates the electron temperature, electron density, and photon density for the next time step.

In the next section, we discuss the hydrogenic option, giving detailed consideration to time-dependent and steady-state ionization balances. We also compare our results for the average ionization state and charge-state abundance with an average-atom model and with the results of recent experimental measurements. In Section III, we discuss the non-hydrogenic option, and use our model to validate a proposed method of estimating ionization-balance data from experimentally measured emission spectra.

II. HYDROGENIC APPROXIMATION

A. Time-Dependent Ionization Balance

In the hydrogenic approximation, the populations for the ground state N_i^1 and excited state N_i^ℓ ($\ell > 1$) of the ion at its i^{th} ionization stage are described by the following equations:

$$\frac{dN_i^\ell}{dt} = - R_i(\ell)N_i^\ell + \sum_k t_i^{\ell k} N_i^k + S_{i+1}(\ell)\, N_{i+1} + \sum_k \left[R_{i-1}(k)\, N_{i-1}^k - S_i(k)\, N_i^1\right] \delta_{\ell,1}, \quad (1)$$

where $t_i^{\ell k} = (n_e\, C_{k\ell}^e + B_{k\ell}\, U_{h\nu}) \qquad \ell > k$,

$$t_i^{\ell k} = (n_e\, C_{k\ell}^d + A_{k\ell} + B_{k\ell}\, U_{h\nu}) \qquad \ell < k \ ,$$

$$t_i^{\ell\ell} = - \sum_{k<\ell} (n_e\, C_{\ell k}^d + A_{\ell k} + B_{\ell k}\, U_{h\nu}) - \sum_{k>\ell} (n_e\, C_{\ell k}^e + B_{\ell k}\, U_{h\nu}) \ ,$$

and n_e = electron density. The symbol $A_{k\ell}$ is the Einstein coefficient for spontaneous emission from state k to state ℓ. The symbol $B_{k\ell}$ is the Einstein stimulated-emission coefficient for a transition induced by radiation of energy density $U_{h\nu}d(h\nu)$ in the energy range from $h\nu$ to $h\nu + d(h\nu)$. The symbol $\delta_{\ell,1}$ stands for the usual delta function, and so is equal to 0 unless $\ell = 1$.

The matrix t_i couples all the energy levels within the i^{th} ionization stage by collisional or radiative transition. $C_{\ell k}^e$ and $C_{k\ell}^d$ are respectively the collisional excitation- and de-excitation-rate coefficients for transitions between level ℓ and level k. The term $R_i(\ell)$ represents the total ionization rate from level ℓ including electron collisional ionization and photoionization. The total recombination rate $S_{i+1}(\ell)$ includes radiative, three-body, and dielectronic recombinations. The term $\sum_k R_{i-1}(k)N_{i-1}^k$ represents the increase of the ground-state population caused by ionization, and the term $\sum_k S_i(k)N_i^1$ represents the decrease of the ground-state population caused by recombination. These two terms exactly cancel each other when the plasma reaches steady-state equilibrium where the total ionization rate of a given ionization stage is equal to the total recombination rate of the higher

ionization stage. Although in this model each excited level is coupled to the ground state of the next ionization stage only, the coupling to the excited state of the next ionization stage is, in general, negligible for electron densities less than 10^{22} cm^{-3}.

The equation for excited state level populations can be rewritten as:

$$\frac{dN_i^{\ell}}{dt} = - R_i(\ell)N_i^{\ell} + \sum_{k>1} \tilde{t}_i^{\ell k} N_i^k + S_{i+1}(\ell) N_{i+1}^1 + (n_e C_{1\ell}^e + B_{1\ell} U_{h\nu}) N_i^1 \qquad \ell > 1 \tag{2}$$

where the matrix $\tilde{t}_i$ couples the excited states together. The symbols $C_{1\ell}^e$ and $B_{1\ell}$ are the electron-collisional excitation-rate coefficients and the radiative-absorption cross section, respectively, for the transition from ground state to level ℓ.

By solving Eq. (2), we obtain the following difference relation for the excited-state level population

$$(N_i^{\ell})^{t+\Delta t} = (c_i^{\ell})^t + \Delta t[a_i^{\ell}(N_i^1)^{t+\Delta t} + b_i^{\ell}(N_{i+1}^1)^{t+\Delta t}] \tag{3}$$

where Δt is the time step for the kinetic calculation. The term c_i^{ℓ} is given in terms of the level populations. Both the coefficients a_i^{ℓ} and b_i^{ℓ} are expressed in terms of the matrix $\tilde{t}_i$ and the ionization- and recombination-rate coefficients.

Substituting Eq. (3) into Eq. (1) gives

$$(N_i^1)^{t+\Delta t} = \left[\Delta t\, F_i^0 + F_i^1 (N_{i-1}^1)^{t+\Delta t} + F_i^3 (N_{i+1}^1)^{t+\Delta t}\right] / (1 - \Delta t\, F_i^2) \tag{4}$$

where the coefficients F_i^0, F_i^1, F_i^2, and F_i^3 depend on a_i^{ℓ}, b_i^{ℓ}, c_i^{ℓ}, and the ionization-rate and recombination-rate coefficients. Equation (4) for the ground-state populations can be solved easily using any method for a tridiagonal matrix.

B. Steady-State Ionization Balance

In steady-state equilibrium, the level populations are determined by the solution of Eq. (1) when dN_i^ℓ/dt is set to zero for every level. Eq. (1) then reduces to the following form:

$$\sum_k \left(T_i^{\ell k}\right) N_i^k = S_{i+1}(\ell)\, N_{i+1}^1 \quad , \tag{5}$$

where

$$T_i^{\ell k} = R_i(\ell)\delta_{\ell k} - t_i^{\ell k} \quad .$$

By solving the level populations in terms of the inverse of the matrix T_i, we have

$$N_i^k = \sum_\ell \left(T_i^{-1}\right)^{k\ell} S_{i+1}(\ell) N_{i+1}^1 \quad . \tag{6}$$

Using these results for the level populations, we write the total ionization rate of the i^{th} ionization stage as

$$\alpha_i N_{i+1}^1 = \sum_{k,\ell} R_i(k)\left(T_i^{-1}\right)^{k\ell} S_{i+}(\ell) N_{i+1}^1 \tag{7}$$

and the total recombination rate for the i+1 ionization stage as

$$\beta_{i+1} N_{i+2}^1 = \left[\sum_k S_{i+1}(k)\right]\left[\sum_\ell \left(T_{i+1}^{-1}\right)^{1\ell} S_{i+2}(\ell)\right] N_{i+2}^1 \, . \tag{8}$$

At steady-state equilibrium, the total ionization rate of the i^{th} ionization stage is exactly equal to the total recombination rate of the i+1 ionization stage. The results are

$$\alpha_i N_{i+1}^1 = \beta_{i+1} N_{i+2}^1 \qquad 1 \le i \le Z_n - 1 \quad , \tag{9}$$

where Z_n = the nuclear charge of the ion.

The excited-state populations are determined by solving Eqs. (6) and (9). The results are

$$N_i^{\ell} = \left[\sum_k (T_i^{-1})^{\ell k} S_{i+1}(k)\right](\beta_{i+1}/\alpha_i)\ (\beta_{i+2}/\alpha_{i+1})\cdots(\beta_{Z_n}/\alpha_{Z_n-1})N_{Z_n+1}, \quad (10)$$

$$N_{Z_n+1} = \frac{t}{1 + \sum_{i\ell k} (T_i^{-1})^{\ell k} S_{i+1}(k)\ (\beta_{i+1}/\alpha_i)(\beta_{i+2}/\alpha_{i+1})\cdots(\beta_{Z_n}/\alpha_{Z_n-1})} ,$$

where N_t is the total ion density and $1 \leq i \leq Z_n$.

If we are interested only in the total population of an ionization stage, we can use Eqs. (6) through (8) to write the total ionization rate as

$$\phi_i N_i = \frac{\alpha_i}{\sum_{\ell k} (T_i^{-1})^{\ell k} S_{i+1}(k)} N_i , \quad (11)$$

and the total recombination rate as

$$\psi_{i+1} N_{i+1} = \frac{\beta_{i+1}}{\sum_{\ell k} (T_{i+1}^{-1})^{\ell k} S_{i+2}(k)} N_{i+1} , \quad (12)$$

where $N_i = \sum_{\ell} N_i^{\ell}$. The total ionization rate, ϕ_i, and the total recombination rate, ψ_i, both depend on the nuclear charge, ionization state, electron temperature, and electron density.

The populations of each ionization stage can be obtained from the following relations:

$$\phi_i N_i = \psi_{i+1} N_{i+1} , \quad 1 \leq i \leq Z_n . \quad (13)$$

The solution for this set of equations is written as

$$N_i = (\psi_{i+1}/\phi_i)(\psi_{i+2}/\phi_{i+1})\cdots(\psi_{Z_n+1}/\phi_{Z_n})\ N_{Z_n+1} , \quad (14)$$

where $N_{Z_n+1} = N_t \Big/ \left[1 + \sum_{i=1}^{Z_n} (\psi_{i+1}/\phi_i)(\psi_{i+2}/\phi_{i+1})\cdots(\psi_{Z_n+1}/\phi_{Z_n})\right]$.

At very high electron density, where the electron collisional de-excitation rate dominates the radiative spontaneous-emission rate, Eq. (13) reduces to the Saha-Boltzmann equilibrium:

$$N_i/N_{i+1} = (G_i n_e \lambda_e^3/2G_{i+1})\, e^{I_i/kT_e} \quad , \tag{15}$$

where $G_i = \sum g_{i,\ell}\, e^{-E_i^{\ell}/kT_e}$,

$g_{i,\ell}$ = statistical weight for level ℓ of i^{th} ionization stage,

E_i^{ℓ} = excitation energy for level ℓ of i^{th} ionization stage,

I_i = ionization potential of i^{th} ionization stage,

T_e = electron temperature, and

λ_e = free electron thermal de-Broglie wavelength.

At very low electron density, where the radiative spontaneous-emission rate dominates the electron collisional de-excitation rate, Eq. (13) reduces to the coronal equilibrium:

$$N_i/N_{i+1} = \sum_{\ell} S_{i+1}(\ell)/R_i(1) \tag{16}$$

where the total recombination rate, $S_{i+1}(\ell)$ includes both radiative and dielectronic recombinations.

C. Atomic Model

Each energy level of an ion is described by a set of occupation numbers $\{P_m\}$. The symbol P_m, which takes on integral values of 0, 1, 2, . . . $2m^2$, gives the number of electrons in the m^{th} shell of the ion. As an example, the ground level of a neon-like ion is characterized by $P_1 = 2$, $P_2 = 8$, $P_m = 0$, $m \geq 3$; the first excited state is characterized by $P_1 = 2$, $P_2 = 7$, $P_3 = 1$, $P_m = 0$, $m \geq 4$. The principal quantum number of a level is determined by its valance electron. This model neglects all the $\Delta n = 0$ transitions and assumes that the sublevels are in statistical equilibrium.

We calculated energy levels for each ionization stage using hydrogenic screening constants. The ionization potential for a level ℓ of the i^{th} ionization stage is taken as

$$I_i^{\ell} = E\,[\{P_m\}_i] - E\,[\{\hat{P}_m\}_{i+1}] \tag{17}$$

where

$$E[\{P_m\}_i] = \sum_m P_m \epsilon(Q_m, m) \quad ,$$

$$Q_m = Z_n - \sum_{n<m} \sigma(m,n)\, P_n - \frac{1}{2}\sigma(m,m)(P_m - 1) \quad , \text{ and}$$

$$\epsilon(Q_m, m) = \frac{1}{2} m_e c^2 \left(\frac{\alpha Q_m}{m}\right)^2 \left[1 + \left(\frac{2m}{m+1} - \frac{3}{4}\right)\left(\frac{\alpha Q_m}{m}\right)^2 + \frac{1}{6}\left(\frac{\alpha Q_m}{m}\right)^4\right]$$

The $\hat{P}_m$ are equivalent to the P_m except for the shell in which an electron is removed by ionization processes. The symbols m_e and c are the electron mass and speed of light, respectively. The term α here represents the fine structure constant, and the term Q_m represents the effective charge of the m-th shell, a value that includes screening from electrons in inner shells only. The binding energy for the m shell, $\epsilon(Q_m, m)$, is calculated using the Pauli approximation to the Dirac equation. The $\sigma(m,n)$ are hydrogenic screening constants.

Several sets of screening constants have been published in the literature. A set derived by Mayer using perturbation theory has been widely used,[3] and while the ionization potentials that are computed based on the Mayer screening constants are reasonably accurate for highly-stripped ions, they are grossly over-estimated for nearly neutral ions.[4] Recently, More has obtained a set of screening constants by least-squares fitting the ionization potentials from the screening model to a data base containing 800 ionization potentials.[2] This new set of screening constants gives satisfactory results for both highly-stripped ions and ions close to neutral. We adapt More's set in our calculation of ground-state ionization potential.

The electron collisional excitation- and ionization-rate coefficients are scaled from the results of Golden and Sampson for hydrogenic ions.[5] The inverse rates are calculated using the detailed balance relation. The Burgess and Merts formula enables us to calculate dielectronic recombination rates for both the $\Delta n = 1$ and $\Delta n = 0$ transitions.[6-7] In calculating the $\Delta n = 0$ transitions, we used Post's values for both the average excitation energy and oscillator strength.[8] The radiative recombination rate is computed from Kramers' classical formula (Ref. 9) together with a bound-free Gaunt factor. The radiative spontaneous-emission rates are calculated using hydrogenic oscillator strengths. All the rate coefficients are represented by simple analytical formulas.

D. Results and Comparison with an Average-Atom Model

Since non-LTE calculations based on an average-atom model have been employed in many laser-produced plasma simulations,[10-12] a comparison with the average ionization states given by our model is of interest. In Fig. 1, we have drawn contour plots showing the ratio of the average ionization state of our model (Z_{DCA}) to an average-atom model (Z_{AA}) in the (T_e,ρ) plane for cesium. These figures represent the results of the average ionization states for an LTE plasma (Fig. 1a) and steady-state optically-thin plasma (Fig. 1b). For $T_e > 20$ eV and $\rho < 1$ g/cm^3, the agreement between models is within 20%. The largest discrepancies occur at high densities and low temperatures, where one expects pressure ionization and multiple excited states to be important. The hydrogenic model, which includes only singly excited electron states, is not expected to be applicable at these temperatures and densities.

Figures 2-6 present the results of the ionization-balance calculations from our model for a steady-state non-LTE plasma. In Fig. 2, we plot the total ionization rate (solid curves) and total recombination rate (dashed curves) for two selenium ionization stages (SeXXIII and SeXXV) as a function of electron temperature at an electron density of 5×10^{20} cm^{-3}. These calculations employ the dielectronic recombination-rate coefficient given by the Burgess-Merts formula. The total ionization rate for neon-like ions becomes equal to the total recombination rate from flourine-like ions at an electron temperature of approximately 1580.0 eV. At this temperature, the neon-like ion population is about equal to the fluorine-like ion population, although it is expected to be greater than the fluorine-like population below 1580.0 eV and less above this temperature.

In Fig. 3, we compare the total ionization rate (solid curve) to the ground-state ionization rate (dashed curve) for SeXXIII and SeXXV ionization stages as a function of electron temperature at an electron density of 5×10^{20} cm^{-3}. The comparison shows the total ionization rate to be greater than that of the ground state by factors of 5 to 10. The enhanced ionization is due to contributions from the excited levels which are populated by collisional excitation from the ground state. Both the collisional excitation rate and the excited-state ionization rate at these temperatures and densities appear large when compared to the ionization rate of the ground state. This condition will result in a charge-state abundance curve which peaks at a lower temperature than a coronal calculation.

In Fig. 4, we plot the average ionization state of a selenium plasma as a function of electron temperature at an electron density of 5×10^{20} cm^{-3}. Also plotted in the figure are the average ionization states given by the LTE and coronal equilibrium models, with the LTE ionization states calculated from the Saha-Boltzmann equation. The coronal model assumes that all the ions in a plasma are in their ground states. The LTE model significantly over-estimates the average ionization state at all temperatures (because these plasmas are not dense enough to be described using the Saha-Boltzmann equation), and the coronal model underestimates the ionization state at low temperature by neglecting excited state ionization. The average ionization state given by our model is generally intermediate between coronal equilibrium and LTE, although the coronal model and our model agree at high electron temperatures where the step-wise ionization contribution is negligible.

In Fig. 5, the charge-state abundances of a hot selenium plasma are plotted as a function of electron temperature at electron densities of 5×10^{18} cm^{-3} (Fig. 5a) and 5×10^{20} cm^{-3} (Fig. 5b). Also plotted in the figures are charge-state abundances given by the coronal equilibrium model (dashed curves). We see that our model agrees with the coronal model at low density (5×10^{18} cm^{-3}), but disagrees by more than one charge state at the higher density (5×10^{20} cm^{-3}). The neon-like ions (Se XXV) dominate the charge-state distribution over a wide range of temperatures because of their closed atomic-shell structure.

In Fig. 6, we plot the charge-state abundance of a hot selenium plasma as a function of electron density at electron temperatures of 500 eV (Fig. 6a) and 1000 eV (Fig 6b). We see that the excited state ionization starts to affect the charge-state abundance at an electron density of 5×10^{18} cm^{-3} at 500 eV and does not contribute to the charge-state abundance until the electron density is 10^{20} cm^{-3} at 1000 eV. This is due to the strong temperature dependence of the ground-state ionization-rate coefficients.

In all of the calculations discussed thus far, we estimated the dielectronic recombination-rate coefficient using the Burgess-Merts formula. To test these rate coefficients, we compared them to a recent detailed calculation[13] which used the Multi-Configuration Dirac-Fock (MCDF) method to compute the Auger and radiative rates of individual doubly-excited states.[14] Figure 7 shows the results of the comparison. We see that our dielectronic recombination-rate coefficient agrees to within 20% of the quantum calculation over a wide range of temperatures.

The effect of dielectronic recombination on the ionization balance of a hot selenium plasma is shown in Fig. 8.

Figure 9 compares the charge-state distribution of a hot steady-state krypton plasma with the distribution measured experimentally.[15] Both the electron temperature and density were estimated using K-shell spectra of phosphorus impurities seeded in the plasmas. The charge-state distribution was inferred from the L- and M-shell emission spectra. Also plotted in the figure are results of a calculation using the code XRASER.[16] Our results agree reasonably well both with the experimental measurement and the XRASER calculation.

Since one of the motivations of our model was to design x-ray laser experiments, we show the results of a prototype Nova exploding-foil target.[17] This design uses a 500-Å Se foil illuminated by a 0.5-μm laser of 400 ps FWHM duration at an intensity of 5×10^{13} W/cm^2. Figure 10a shows the LASNEX (T_e,n_e) time histories that result from laser illumination. The electron temperature and density are approximately 900 eV and 5×10^{20} cm^{-3}, respectively, at the peak of the laser pulse. In Fig. 10b, we show the charge-state distribution, which has reached steady state by the peak of the laser (roughly 0.75 ns). Finally, in Fig. 10c we compare the output x-ray energy of the average atom (AA) to the result given by our model (DCA). Although the integrated outputs agree to within 10%, our results obviously provide additional details in the photon energy range below 1 keV that are important in interpreting experimental results.

In Fig. 11, we plot the radiative cooling rates of an optically thin selenium plasma as a function of electron temperature at an electron density of 5×10^{20} cm^{-3}. The individual contributions from bound-bound (line), bound-free (recombination), and free-free (bremsstrahlung) radiations are plotted separately. At low electron temperature, the line emission is totally dominant, but bremsstrahlung becomes dominant at a temperature of about 20 keV. Radiative recombination does not contribute significantly to the total radiative cooling rate at these electron densities. Our calculation neglects the line emission from $\Delta n = 0$ transitions because their contribution to the total radiative cooling rate is in general negligible at densities of 10^{20} cm^{-3}.

III. NON-HYDROGENIC APPROXIMATION

A. Basic Equations

Our model obtains the level populations for the ionization stages which are described using non-hydrogenic atomic data from the solution of the following rate equations:

$$\frac{dN_\ell}{dt} + \sum_k (W_{k\ell}\, N_\ell - W_{\ell k}\, N_k) = S_\ell \qquad (18)$$

where $W_{\ell k}$ are the collisional and radiative rates for the transition between levels ℓ and k. The term S_ℓ gives the contribution to the population of level ℓ that is caused by either ionization or recombination from other ionization stages (not included in the equation). The summation runs over all the levels in the non-hydrogenic ionization stages. The level populations for the rest of the ionization stages are calculated using Eqs. (3) and (4) in the hydrogenic approximation.

The model reads an atomic data file to obtain the energy levels, statistical weights, oscillator strengths, electron collisional excitation- and ionization-rate coefficients, photoionization cross sections, and autoionization rates. The rate coefficients and cross sections are fit to simple analytic expressions and the fitting coefficients are stored in the data file.

These data files (which are also read by other x-ray laser design codes such as XRASER) are generated by a computer package called ADAM.[18] Briefly, ADAM receives the content of the model to be made from a generator deck and then creates a model either from an atomic physics data base or from simple analytic formulas. The data base contains primary atomic data which could be obtained from experimental measurement or more elaborate atomic code calculation.

This last option makes it possible to apply the model to the analysis of non-LTE emission spectra and to the design of laboratory x-ray laser experiments.

B. Results and Discussion

Figure 12 shows the charge-state distribution of a selenium plasma at an electron density of 5×10^{20} cm^{-3} and electron temperature of 1000 eV. The solid curve represents the results of a calculation using the default hydrogenic option of our model, the dashed curve represents the results for an atomic model which treats the neon-like ionization stage in non-hydrogenic approximation, and the dotted curve represents the results for an atomic model which treats both Ne- and F-like ionization stages in non-hydrogenic approximation. The atomic model has 58 energy levels for the Ne-like ion and 113 energy levels for the F-like ion.

The energy levels for the $n = 2$ and $n = 3$ states of Ne- and F-like ions are computed using the multi-configuration Dirac-Fock code YODA.[19] The oscillator strengths for the transitions between these states are also computed using YODA.

Figure 13 shows the average ionization state of a selenium plasma at an electron density of 5×10^{20} cm^{-3} as a function of electron temperature. These comparisons in Figs. 12 and 13 show that the calculation using a hydrogenic model produces results which agree reasonably well with calculations using a more detailed atomic model.

C. Ionization Balance Derived from Emission Spectra

In this section we use our model to validate a proposed method of measuring ionic charge-state abundance in non-LTE plasmas. This method obtains the ratio of populations for two ionization stages from the relative intensities of the integrated x-ray flux in the spectral lines between two configurations seen in both kinds of ions that are produced in a plasma. For example, the ratio of populations for Ne-like ions to F-like ions is measured by comparing the relative spectral line intensities arising from the 2p - 3d transitions of such ions and scaling the relative intensities to the number of 2p electrons in each ion. This method assumes that the 3d-level populations are dominantly produced by electron-collisional excitation from the ground state. We have estimated the cascade contribution to the 3d-level populations in both F-like and Ne-like ions to be less than 20% for most laboratory plasmas that are produced using a z-pinch or a high-power laser.

Stewart[15] has applied this methoc together with a satellite line model for Ne-like ions to measure the krypton charge-state distribution in plasmas that are produced using a z-pinch. The results of his measurement have already been plotted in Fig. (9), together with the results of our calculation. Recently, Bailey[20] used the same method to measure ionic charge-state abundance of Ni-, Co-, and Fe-like ions in europium plasmas produced with laser-irradiated micro-dot targets.

To test this method for measuring ionization balance in non-LTE plasmas, we calculated all the spectral line intensities arising from the 2p - 3d transitions in Ne-like and F-like selenium ions. We then used these relative intensities to compute the ratio of populations for Ne-like ions to F-like ions. Results are plotted in Fig. 14 together with the ratio of populations predicated by our model. We see that the population ratios obtained from the relative intensities of 2p - 3d transitions agree to within 20% of the results given by the ionization-balance model over a wide range of electron temperatures and densities. This agreement suggests that ionization balance can be measured by comparing relative intensities for a set of the transitions seen in each ionization stage.

IV. SUMMARY

We have developed a detailed configuration-accounting kinetic model for calculating time-dependent ionization balance and ion-level populations in non-LTE plasmas. The model offers two options for calculating level populations. The default option treats all the ionization stages in hydrogenic approximation and applies analytical formulae to the calculation of rate coefficients for both collisional and radiative transitions. The second option treats certain ionization stages in non-hydrogenic approximation. The model gathers all of the atomic data for these ionization stages from a data-file. The second option allows one to use the model in simulating x-ray laser and plasma-spectroscopy experiments.

We have also coupled the model self-consistently to the hydrodynamics code LASNEX. After obtaining the electron density and temperature and photon intensity from LASNEX, the model computes the time-dependent level populations. Next the average ionization state, emissivity, photon cross section, and binding energy are computed using these new level populations. LASNEX introduces these quantities into the equation of hydrodynamics, photon transport, and conservation of energy

References

1. G. B. Zimmerman, Lawrence Livermore National Laboratory, Livermore, Calif., UCRL-74811 (1973). Also published in 1984 Laser Program Annual Report, Lawrence Livermore National Laboratory, Livermore, Calif., UCRL-50021-84 (1984).

2. R. M. More, Lawrence Livermore National Laboratory, Livermore, Calif., UCRL-84991 (1982).

3. H. Mayer, Los Alamos Scientific Laboratory, Report No. LA-647 (1947).

4. R. M. More, H-Division Quarterly Report, Lawrence Livermore National Laboratory, Livermore, Calif., UCRL-50028-79-2 (1979).

5. L. Golden and D. Sampson, Astrophys. J. **170**, 181 (1971).

6. A. Burgess, Astrophys. J. **141**, 1588 (1965).

7. A. L. Merts, R. D. Cowan, and N. H. Magee, Jr., Los Alamos National Laboratory, NM, LA-6220-MS (1976).

8. D. E. Post, R. V. Jenen, C. B. Tarter, W. H. Grasberger, and W. A. Lokke, At. Data Nucl. Table **20** 239 (1977).

9. H. A. Kramer, Phil. Mag. **271**, 836 (1923).

10. W. A. Lokke and W. H. Grasberger, Lawrence Livermore National Laboratory, Livermore, Calif., UCRL-52276 (1977).

11. M. Rosen, D. Phillion, V. Rupert, W. Mead, W. Kruer, J. Thompson, H. Kornblum, V. Slivinsky, G. Caporaso, M. Boyle, and K. Tirsel, Phys. of Fluids **22** 2020 (1979).

12. T. Yabe and C. Yamanaka, Comments Plasma Physics, Controlled Fusion, 1, No. 4, 169, (1985).

13. M. Chen, Lawrence Livermore National Laboratory, Livermore, Calif., private communication (1985).

14. I. Grant, J. Phys. B9, 2777 (1976)

15. R. E. Stewart, Ph.D. dissertation, University of California, Davis (1985) (unpublished).

16. P. L. Hagelstein, Lawrence Livermore National Laboratory, Livermore, Calif., UCRL-53100 (1981).

17. M. Rosen, Lawrence Livermore National Laboratory, Livermore, Calif., private communication (1985).

18. J. K. Nash, W. L. Morgan, R. K. Jung, and D. R. Kim, (to be published later in 1986 in the Proceedings of Third International Conference on Radiative Properties of Hot Dense Matter, Williamsburg, Va., October 14-18, 1985).

19. P. L. Hagelstein and R. K. Jung, unpublished (1985).

20. J. Bailey, Sandia National Laboratories, Albuquerque, NM (private communication).

Figures

Figure 1a Contour plot of Z_{DCA}/Z_{AA}, the ratio of the average ionization of our model to an average-atom model for an LTE cesium plasma in (T_e,ρ) space.

Figure 1b Contour plot of Z_{DCA}/Z_{AA} for a steady-state optically-thin cesium plasma in (T_e,ρ) space.

Figure 2 Total ionization rate (solid curves) and recombination rate (dashed curves) as a function of electron temperature for a selenium plasma at an electron density of $n_e = 5 \times 10^{20}$ cm^{-3}.

Figure 3 Comparison of the total ionization rate (solid curves) to the ground-state ionization rate (dashed curves) for a selenium plasma ($n_e = 5 \times 10^{20}$ cm^{-3}).

Figure 4 Three kinetic models of the average ionization state of a selenium plasma as a function of electron temperature ($n_e = 5 \times 10^{20}$ cm^{-3}).

Figure 5a Present model (solid curves) and the coronal equilibrium model (dashed curves) of the charge-state abundance of selenium as a function of electron temperature ($n_e = 5 \times 10^{18}$ cm^{-3}).

Figure 5b A similar comparison to that shown in Figure 5a of charge-state abundance versus electron temperature at a different electron density ($n_e = 5 \times 10^{20}$ cm^{-3}).

Figure 6a Charge-state abundance versus electron density at an electron temperature of $T_e = 500$ eV.

Figure 6b Charge-state abundance versus electron density at $T_e = 1000$ eV.

Figure 7 Comparison of the dielectronic recombination-rate coefficient (calculated using the Burgess-Merts formula) with a recent calculation using the Multi-Configuration Dirac-Fock Method (MCDF).

Figure 8 Dependence of the charge-state abundance of a selenium plasma on the dielectronic recombination-rate coefficients. The symbol γ is the dielectronic recombination multiplier. The electron density $n_e = 5 \times 10^{20}$ cm^{-3} and the temperature T_e = 1000 eV.

Figure 9 Charge-state distribution for a krypton plasma at an electron temperature of 800 eV and an electron density of 3×10^{20} cm^{-3}.

Figure 10a Time histories of electron temperature (T_e) and density (n_e) for two zones of an x-ray laser exploding-foil-target design.

Figure 10b Time dependence of charge states SeXXIII to SeXXVII for an x-ray laser foil-target design.

Figure 10c Comparison of our model (DCA calculation) and an average-atom (AA) model output spectrum for an x-ray laser foil-target design.

Figure 11 Radiative cooling rate for an optically thin selenium plasma as a function of electron temperature at $n_e = 5 \times 10^{20}$ cm^{-3}. The bound-bound (lines), bound-free (recombination) and free-free (bremsstrahlung) radiation contributions are plotted separately.

Figure 12 Charge-state distributions of a selenium plasma calculated using three different atomic models at $n_e = 5 \times 10^{20}$ cm^{-3} and T_e = 1000 eV. The solid line represents the hydrogenic model, the dashed line incorporates the non-hydrogenic approximation for SeXXV and SeXXVI, and the dotted line uses the non-hydrogenic approximation for SeXXV.

Figure 13 Average ionization states versus electron temperature of selenium plasmas calculated with two different atomic models at n_e = 5×10^{20} cm^{-3}. The solid curve again represents the hydrogenic model, and the non-hydrogenic approximation for SeXXV and SeXXVI is given by the data points (o).

Figure 14 Ratio of populations for Ne-like selenium ions to F-like selenium ions versus electron temperature at electron densities of 10^{20} cm^{-3} and 10^{21} cm^{-3}. The solid curves represent results given by the ionization-balance model. The dashed curves represent results obtained by comparing the relative intensities of 2p - 3d transitions that are seen in each ionization stage.

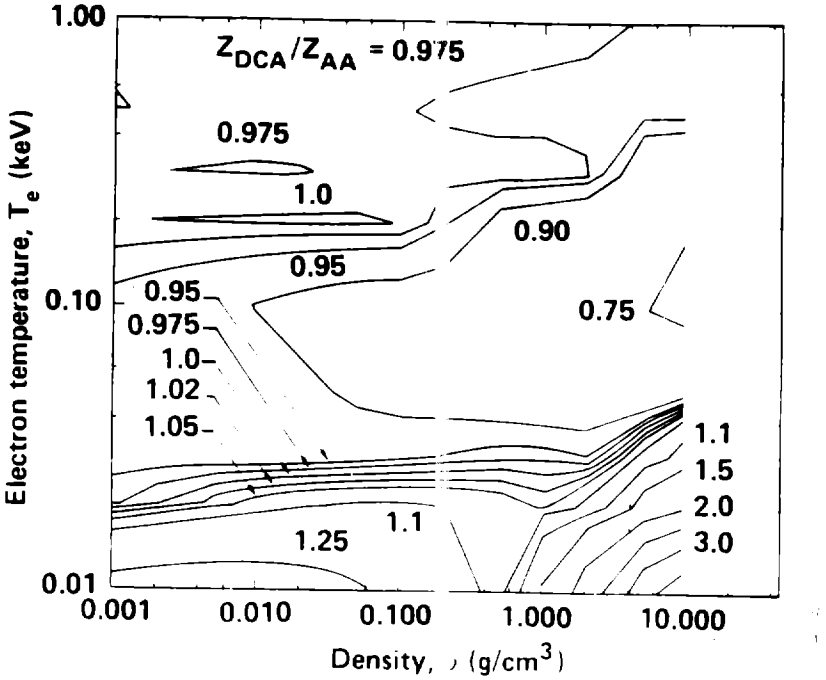
1.00
0.10
0.01
Electron temperature, T_e (keV)
Z_{DCA}/Z_{AA} = 0.975
0.975
1.0
0.90
0.95
0.95
0.975
1.0
1.02
1.05
0.75
1.1
1.5
2.0
3.0
1.1
1.25
0.001
0.010
0.100
1.000
10.000
Density, ρ (g/cm^3)

Lee - Fig. 1a

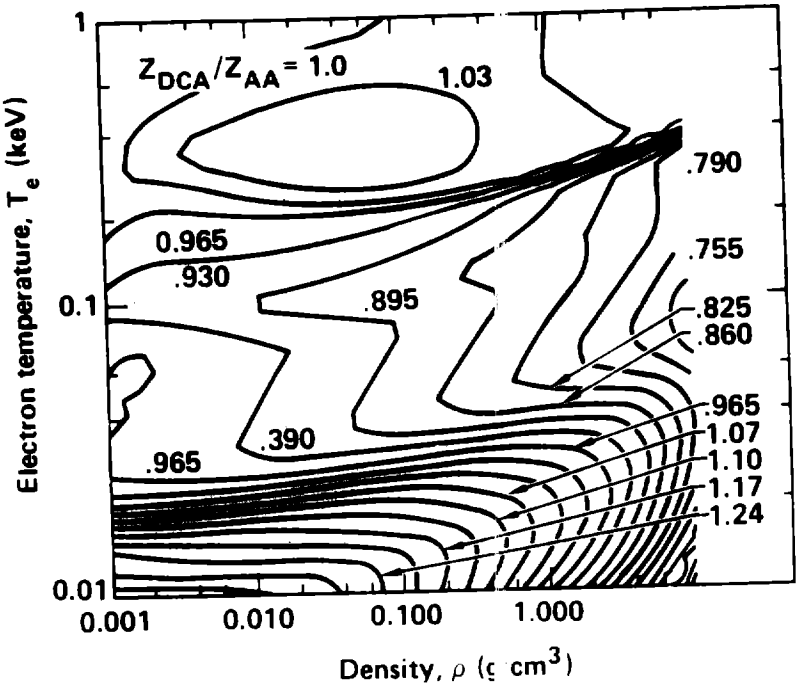
1
0.1
0.01
0.001
0.010
0.100
1.000
Electron temperature, T_e (keV)
Density, ρ (g cm^3)
Z_{DCA}/Z_{AA} = 1.0
1.03
.790
.755
.825
.860
0.965
.930
.895
.965
.390
.965
1.07
1.10
1.17
1.24

Lee - Fig. 1b

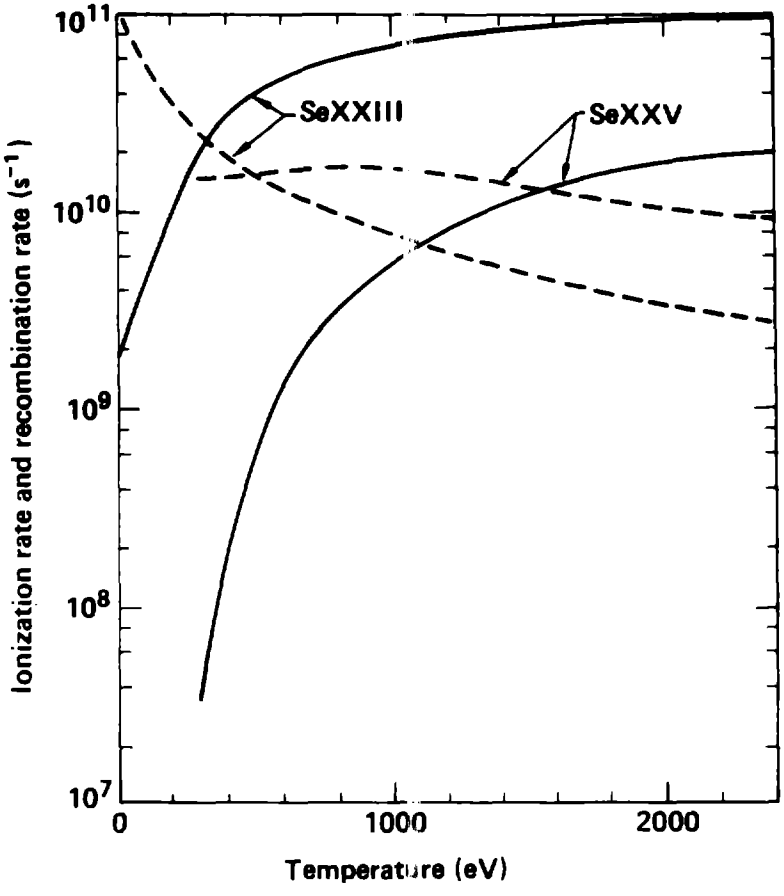
10^{11}
10^{10}
10^{9}
10^{8}
10^{7}
Ionization rate and recombination rate (s^{-1})
SeXXIII
SeXXV
0
1000
2000
Temperature (eV)

Lee - Fig. 2

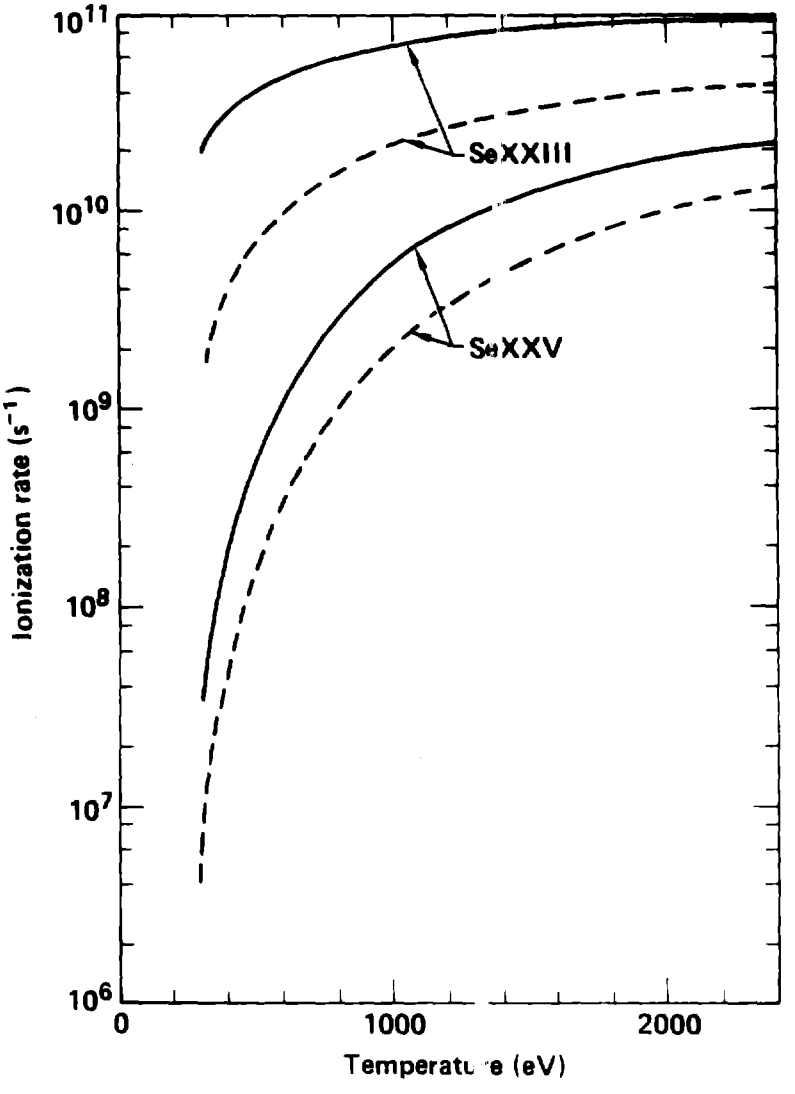
10^{11}
10^{10}
10^{9}
10^{8}
10^{7}
10^{6}
Ionization rate (s^{-1})
SeXXIII
SeXXV
0
1000
2000
Temperature (eV)

Lee - Fig. 3

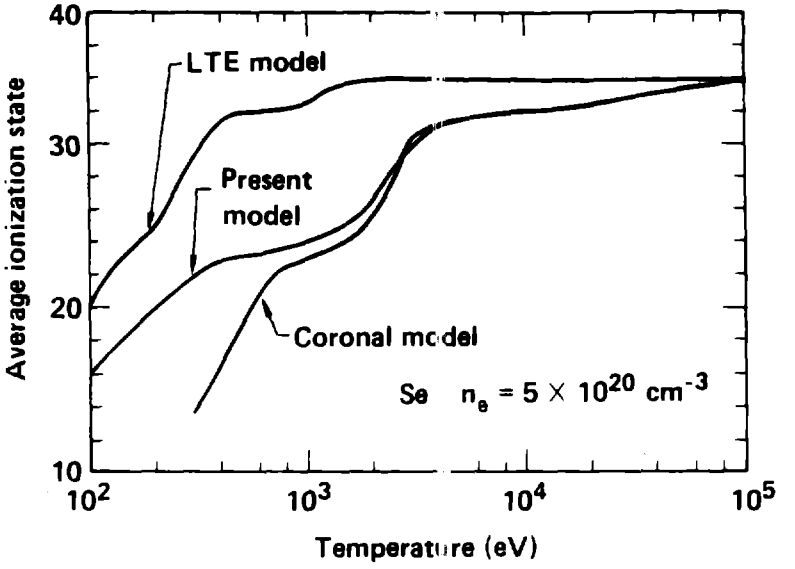
40
30
20
10
LTE model
Present
model
Coronal model
Se $n_e = 5 \times 10^{20}$ cm^{-3}
Average ionization state
10^2
10^3
10^4
10^5
Temperature (eV)

Lee - Fig. 4

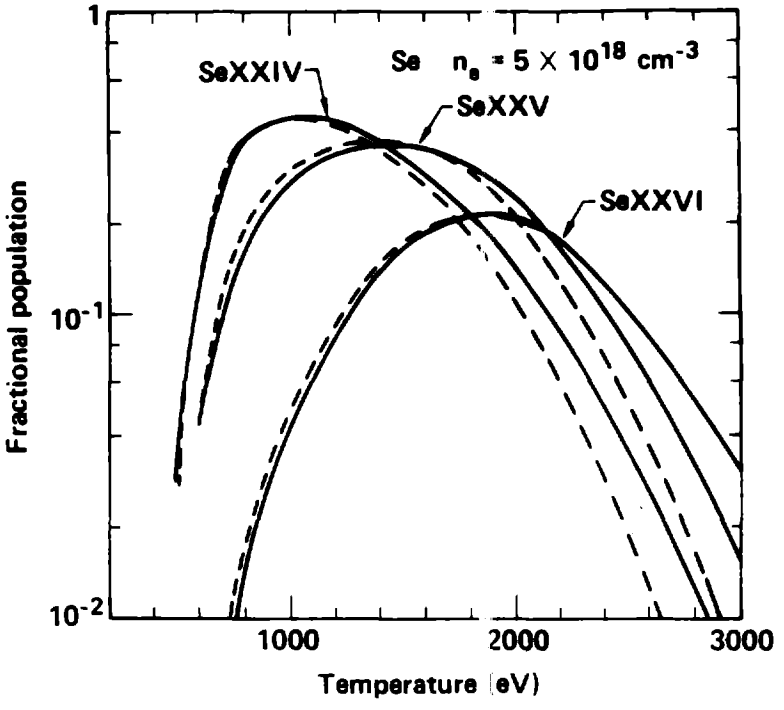
1
10^{-1}
10^{-2}
Fractional population
Se $n_e = 5 \times 10^{18}$ cm^{-3}
SeXXIV
SeXXV
SeXXVI
1000
2000
3000
Temperature (eV)

Lee - Fig. 5a

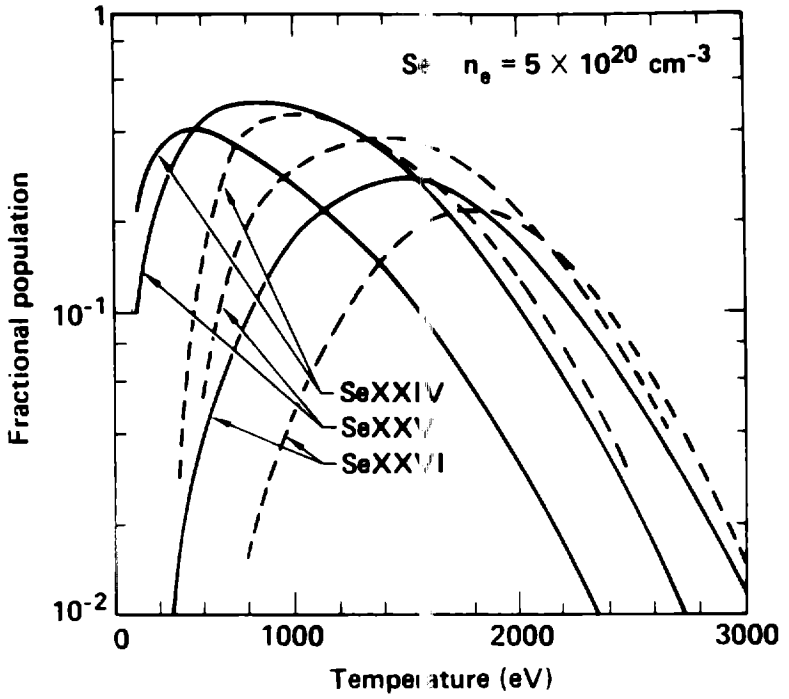
Se $n_e = 5 \times 10^{20}$ cm^{-3}
Fractional population
1
10^{-1}
10^{-2}
SeXXIV
SeXXV
SeXXVI
0
1000
2000
3000
Temperature (eV)

Lee - Fig. 5b

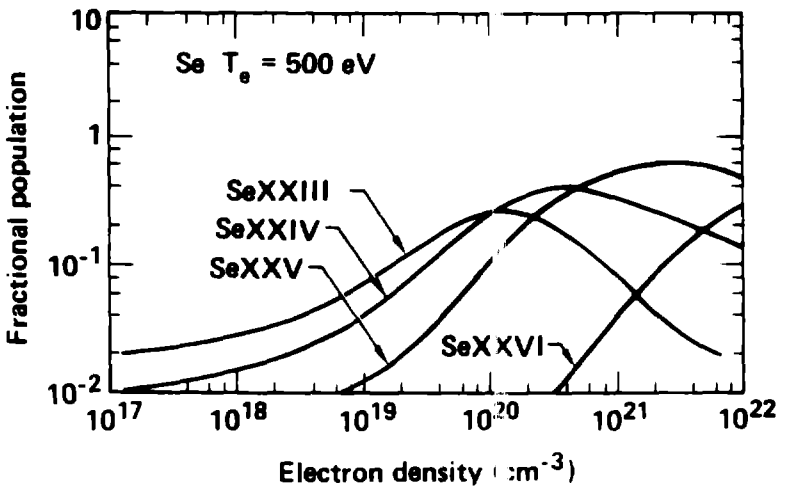
Se T_e = 500 eV
SeXXIII
SeXXIV
SeXXV
SeXXVI
Fractional population
10
1
10^{-1}
10^{-2}
10^{17}
10^{18}
10^{19}
10^{20}
10^{21}
10^{22}
Electron density (:m^{-3})

Lee - Fig. 6a

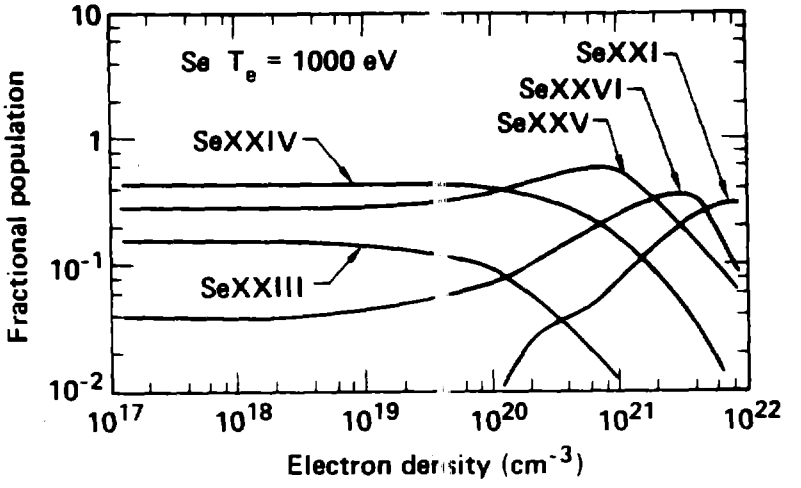
Se T_e = 1000 eV
SeXXI
SeXXVI
SeXXV
SeXXIV
SeXXIII
Fractional population
10
1
10^{-1}
10^{-2}
10^{17}
10^{18}
10^{19}
10^{20}
10^{21}
10^{22}
Electron density (cm^{-3})

Lee - Fig. 6b

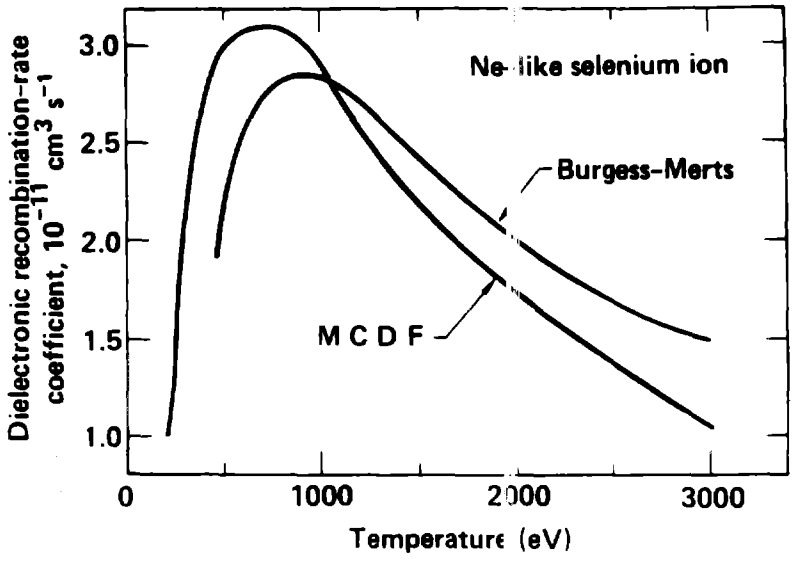
Dielectronic recombination-rate coefficient, 10^{-11} cm^3 s^{-1}
3.0
2.5
2.0
1.5
1.0
0
1000
2000
3000
Temperature (eV)
Ne-like selenium ion
Burgess-Merts
M C D F

Lee - Fig. 7

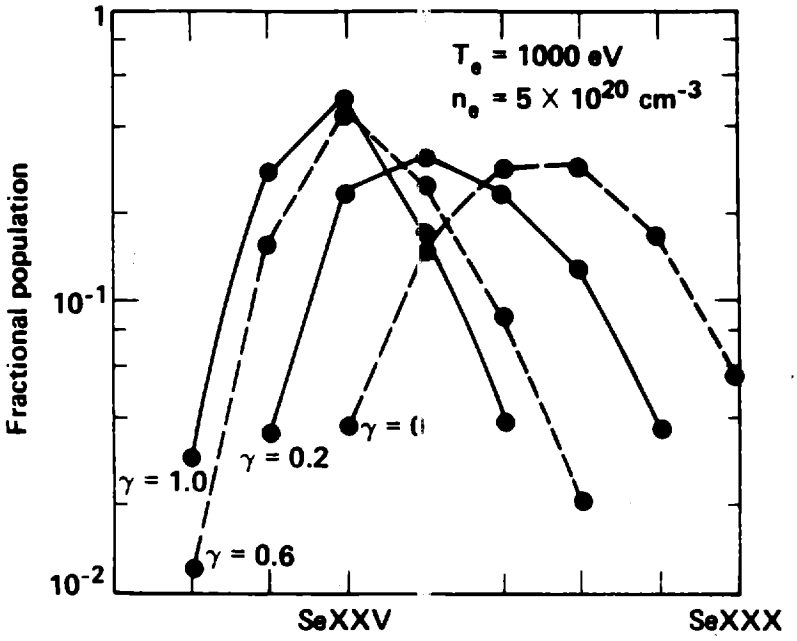
1
10^{-1}
10^{-2}
Fractional population
T_e = 1000 eV
n_e = 5 X 10^{20} cm^{-3}
γ = 1.0
γ = 0.6
γ = 0.2
γ = 0
SeXXV
SeXXX

Lee - Fig. 8

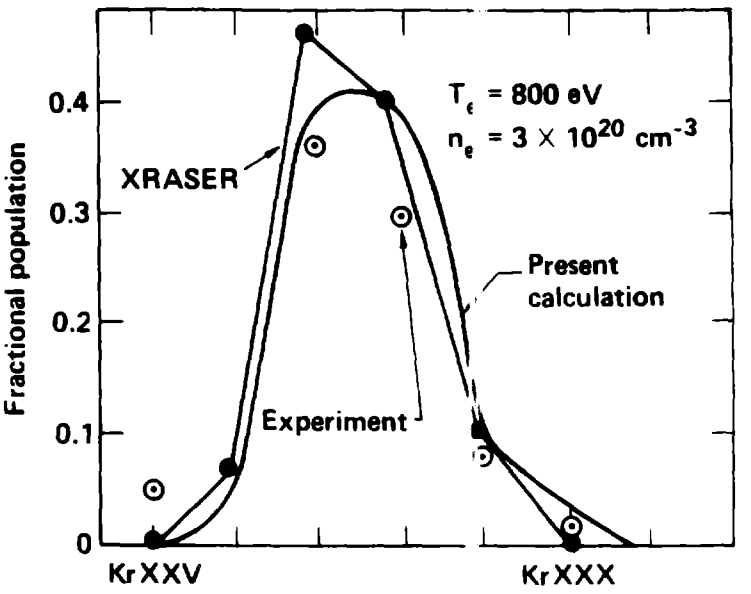
Fractional population
0.4
0.3
0.2
0.1
0
T_e = 800 eV
n_e = 3 × 10^{20} cm^{-3}
XRASER
Present calculation
Experiment
KrXXV
KrXXX

Lee - Fig. 9

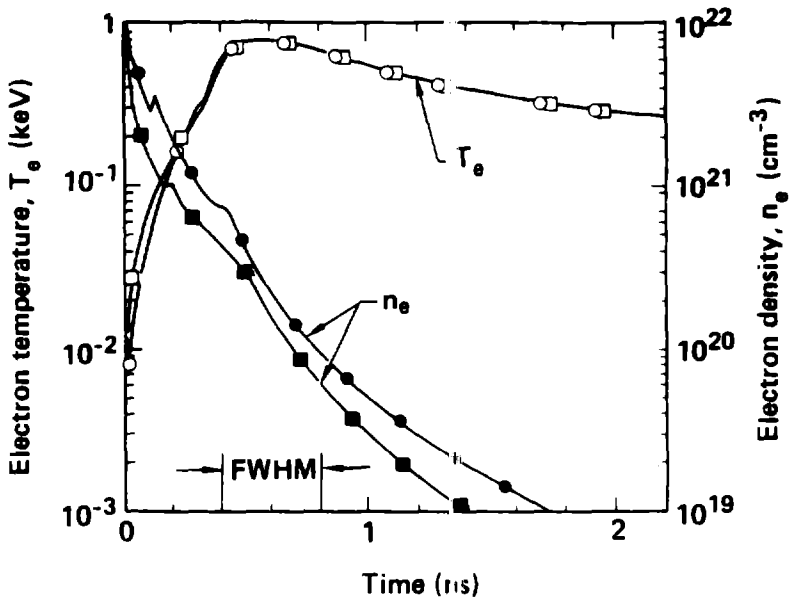
Electron temperature, T_e (keV)
Electron density, n_e (cm^{-3})
Time (ns)
T_e
n_e
FWHM
1
10^{-1}
10^{-2}
10^{-3}
10^{22}
10^{21}
10^{20}
10^{19}
0
1
2

Lee - Fig. 10a

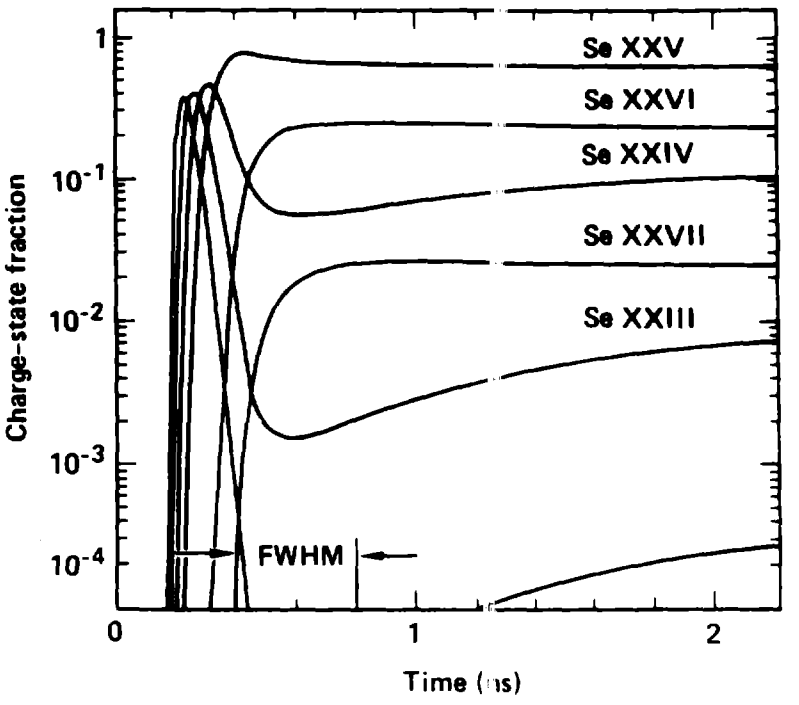
Charge-state fraction
1
10^{-1}
10^{-2}
10^{-3}
10^{-4}
Se XXV
Se XXVI
Se XXIV
Se XXVII
Se XXIII
FWHM
0
1
2
Time (ns)

Lee - Fig. 10b

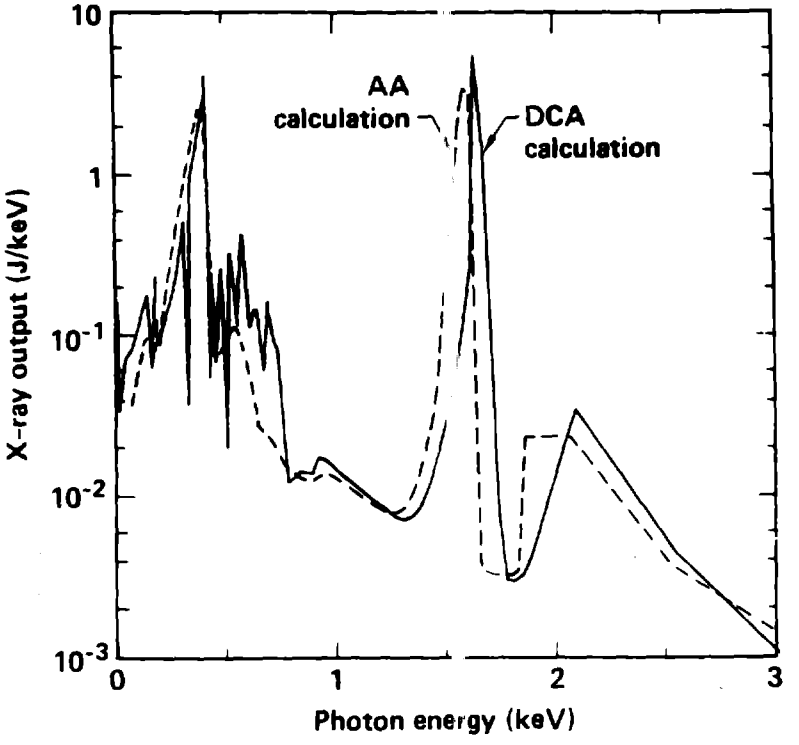
10
1
10^{-1}
10^{-2}
10^{-3}
X-ray output (J/keV)
AA
calculation
DCA
calculation
0
1
2
3
Photon energy (keV)

Lee - Fig. 10c

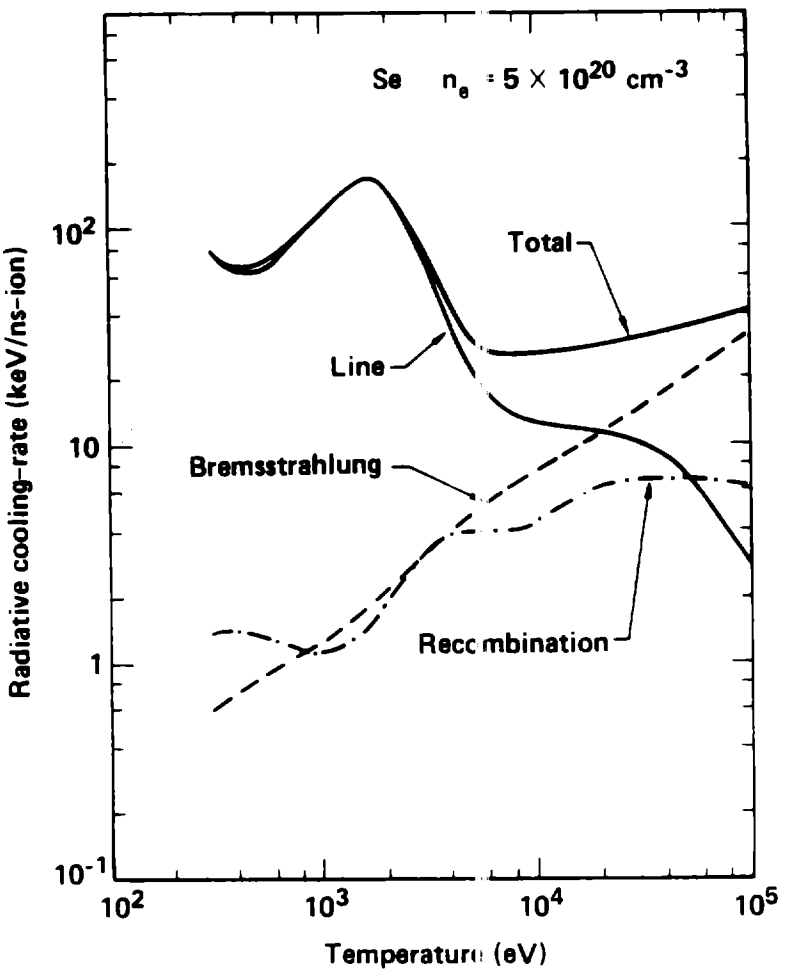
Se $n_e = 5 \times 10^{20}$ cm^{-3}
Total
Line
Bremsstrahlung
Recombination
Radiative cooling-rate (keV/ns-ion)
10^2
10
1
10^{-1}
10^2
10^3
10^4
10^5
Temperature (eV)

Lee - Fig. 11

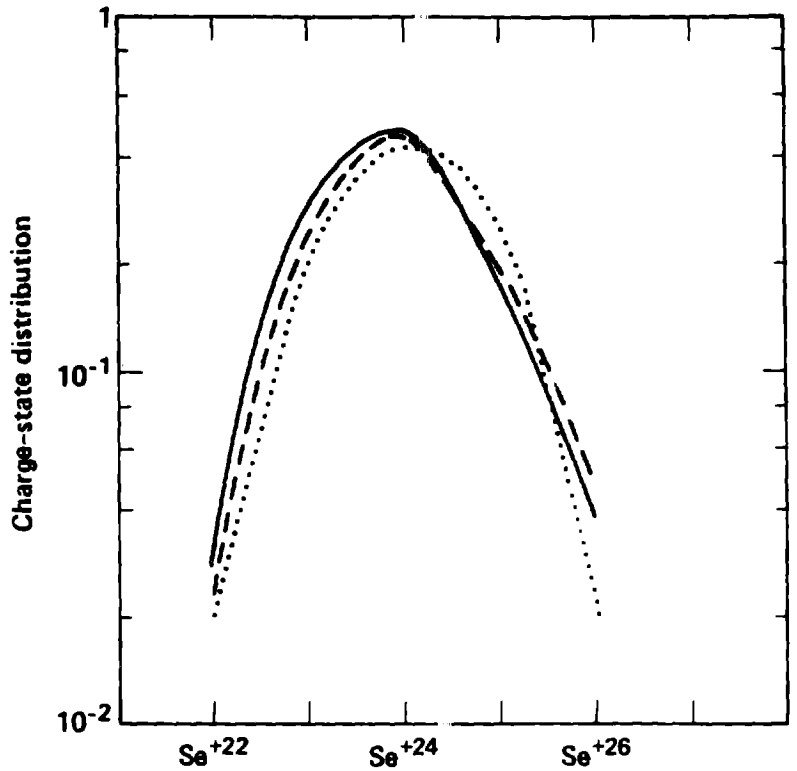

Lee - Fig. 12

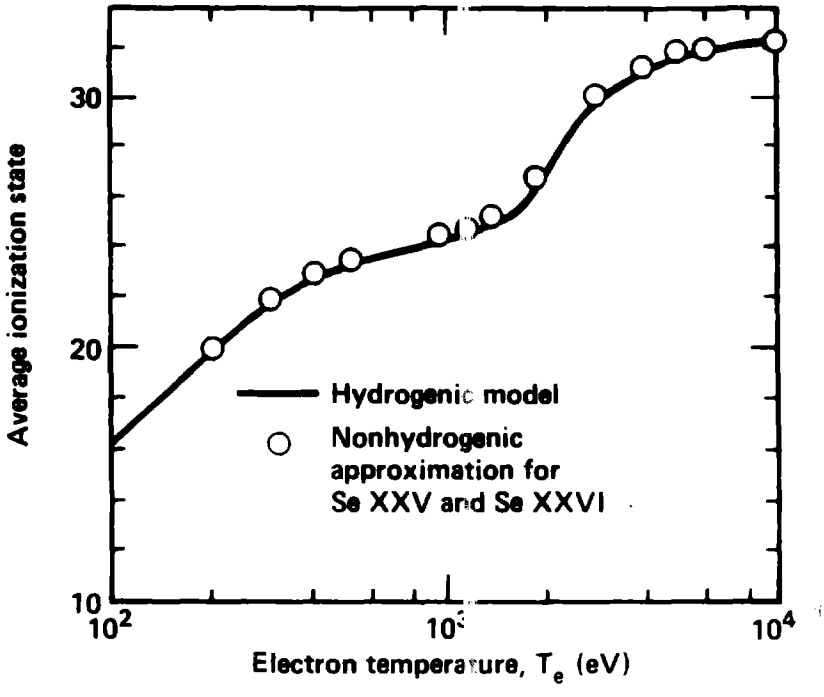
Average ionization state
30
20
10
10^2
10^4
Electron temperature, T_e (eV)
Hydrogenic model
Nonhydrogenic approximation for Se XXV and Se XXVI

Lee - Fig. 13

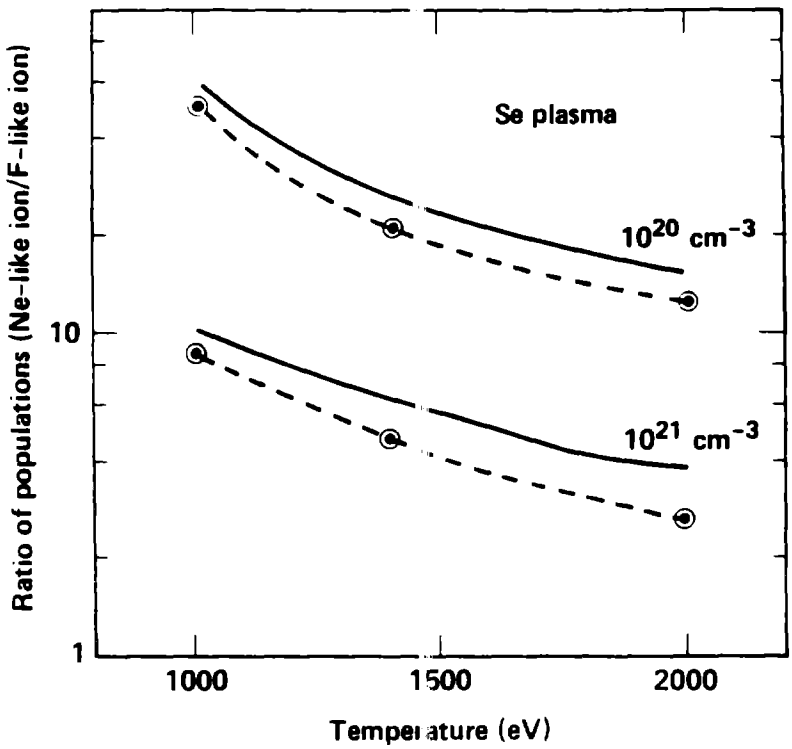
Se plasma
10^{20} cm^{-3}
10^{21} cm^{-3}
Ratio of populations (Ne-like ion/F-like ion)
10
1
1000
1500
2000
Temperature (eV)

Lee - Fig. 14